© 2018. Published by The Company of Biologists Ltd | Development (2018) 145, dev159095. doi:10.1242/dev.159095

STEM CELLS AND REGENERATION

RESEARCH ARTICLE

Intrahepatic bile ducts guide establishment of the intrahepatic nerve network in developing and regenerating mouse liver

Naoki Tanimizu*, Norihisa Ichinohe and Toshihiro Mitaka

ABSTRACT

Epithelial organs consist of multiple tissue structures, such as epithelial sheets, blood vessels and nerves, which are spatially organized to achieve optimal physiological functions. The hepatic nervous system has been implicated in physiological functions and regeneration of the liver. However, the processes of development and reconstruction of the intrahepatic nerve network and its underlying mechanisms remain unknown. Here, we demonstrate that neural class III β-tubulin (TUBB3)$^+$ nerve fibers are not distributed in intrahepatic tissue at embryonic day 17.5; instead, they gradually extend along the periportal tissue, including intrahepatic bile ducts (IHBDs), after birth. Nerve growth factor (*Ngf*) expression increased in biliary epithelial cells (BECs) and mesenchymal cells next to BECs before nerve fiber extension, and *Ngf* was upregulated by hairy enhancer of slit 1 (Hes family bHLH transcription factor 1; Hes1). Ectopic NGF expression in mature hepatocytes induced nerve fiber extension into the parenchymal region, from where these fibers are normally excluded. Furthermore, after BECs were damaged by the administration of 4,4-diaminodiphenylmethane, the nerve network appeared shrunken; however, it was reconstructed after IHBD regeneration, which depended on the NGF signal. These results suggest that IHBDs guide the extension of nerve fibers by secreting NGF during nerve fiber development and regeneration.

KEY WORDS: Nerve network, Intrahepatic bile duct, Neurotrophic factor, Liver, Epithelial tubules

INTRODUCTION

Autonomic nerves form networks throughout the body and regulate many types of physiological process. For example, during the development of epithelial tissues and organs, autonomic nerve fibers establish an organized spatial arrangement with blood vessels and epithelial structures (Carmeliet and Tessier-Lavigne, 2005; Lu and Werb, 2008). In developing skin, sensory nerves guide vascular branching and induce arterial differentiation by secreting chemokine (C-X-C motif) ligand 12 (CXCL12) and vascular endothelial growth factor (VEGF)-A, respectively (Li et al., 2013). In the developing gut, arterial vascular smooth muscle cells facilitate sympathetic innervation of the gut arteries by secreting netrin-1 (Brunet et al., 2014). In submandibular glands, epithelial progenitors secrete WNTs and promote the establishment of neuro-epithelial interactions, which are necessary for both innervation of the tissue and the maintenance of progenitor cells (Knosp et al., 2015). In salivary glands, parasympathetic nerves promote ductal growth by secreting vasoactive intestinal peptide and also induce lumen expansion (Nedvetsky et al., 2014). These results suggest that, in addition to neuro-vascular interactions, neuro-epithelial interactions are important for tissue morphogenesis. However, the processes that establish neuro-epithelial interactions and the molecular mechanisms that regulate these interactions during development and regeneration remain unknown in most epithelial tissues and organs.

The liver is an important organ that performs various physiological functions, including carbohydrate and lipid metabolism, production of serum proteins, detoxification of ammonia and protection from pathogens. These diverse functions are achieved by correct spatial arrangements among tissue structures, including hepatic cords, intrahepatic bile ducts (IHBDs), portal and central veins (PVs and CVs), hepatic arteries (HAs), sinusoids and nerve networks. It has been demonstrated that nerve fibers are restricted within the Glisson's sheath in rats, whereas they extend into the parenchymal region in humans and guinea pigs (Fukuda et al., 1996). It is assumed that the abundance of gap junctions between hepatocytes compensates for the lack of direct innervation in rats (Seseke et al., 1992). The hepatic nerve system has been implicated in the regulation of metabolism, of blood volume in the liver and of bile secretion as well as of tissue repair and regeneration (Shimazu and Fukuda, 1965; Shimazu and Amakawa, 1968; Kato and Shimazu, 1983; Barja and Mathison, 1984; Alvaro et al., 1997; Cox et al., 2004; Ueno et al., 2004). However, it remains unknown how the intrahepatic nerve network is established and reconstructed during liver organogenesis and regeneration.

In this work, we used two-dimensional (2D) and three-dimensional (3D) approaches to examine the nerve network in the developing and regenerating mouse liver, and then correlated the formation of the intrahepatic nerve network with tubular morphogenesis of IHBDs. We also identified NGF secreted from EpCAM$^+$ biliary epithelial cells (BECs) and Thy1$^+$ mesenchymal cells (MCs) next to BECs, which are epithelial and mesenchymal components of IHBDs, respectively, as a crucial factor for the establishment of the neural network in the developing and regenerating liver.

RESULTS

The nerve network in mouse adult liver

Nerve fibers have been observed in the Glisson's sheath but not in the parenchymal region in rat livers, whereas they extend into the parenchymal region and may form direct contacts with stellate cells and sinusoidal endothelial cells (ECs) in humans (Jensen et al., 2013). To determine whether the intrahepatic nerve network in mice resembles that of either rats or humans, we first examined the localization of nerve fibers in adult mouse liver tissue sections (Fig. 1A). Thick nerve fibers recognized by anti-neural class III β-

Department of Tissue Development and Regeneration, Research Institute for Frontier Medicine, Sapporo Medical University School of Medicine, S-1, W-17, Chuo-ku, Sapporo 060-8556, Japan.

*Author for correspondence (tanimizu@sapmed.ac.jp)

N.T., 0000-0001-8167-1401

Received 1 September 2017; Accepted 23 March 2018

Development (2018) 145, dev159095. doi:10.1242/dev.159095

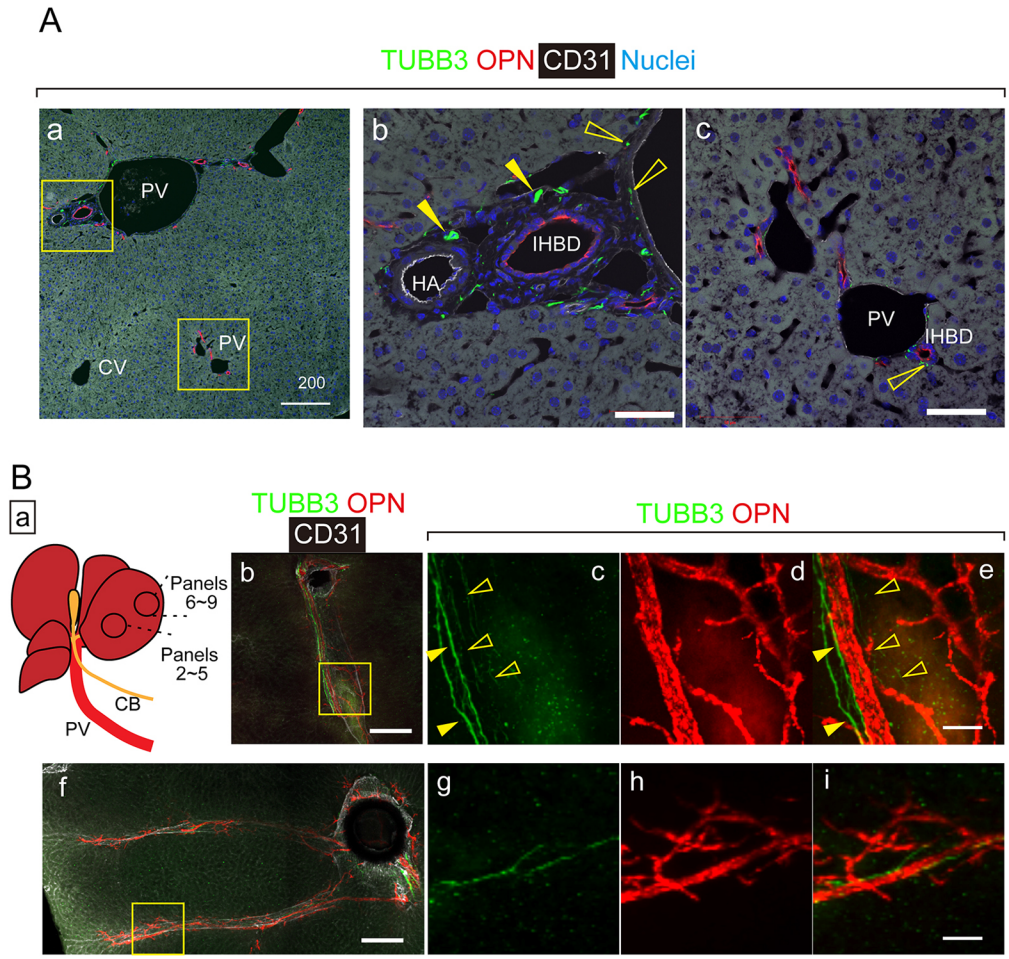

Fig. 1. Intrahepatic nerve network in the adult liver. (A) Localization of nerve fibers, IHBDs and blood vessels in the adult liver. Thick nerve fibers positive for neural TUBB3 are localized near a large IHBD and a HA (b, closed arrowheads), whereas fine nerve fibers are evident around the PV (b, open arrowheads). In the periphery, IHBDs are associated with fine nerve fibers (c, open arrowheads). Hepatic arteries are not clearly recognized in this region. Nerves, IHBDs and blood vessels were recognized by anti-TUBB3, anti-OPN and anti-CD31 antibodies, respectively. Sections prepared from three mice were used for immunostaining and representative data are shown in this figure. Boxes in panel a are enlarged in b,c. (B) IHBDs are thoroughly associated with nerve fibers throughout liver tissue. IHBDs and the nerve network were examined near the hilum and the peripheral region (a). Two thick nerve fibers run along a large IHBD tubule (c,e, closed arrowheads). Fine nerve fibers exist around the PV (c,e, open arrowheads). Even in peripheral liver tissue, nerve fibers run along bile duct tubules. Adult liver tissue blocks were incubated with antibodies and then cleared in SCALEVIEW-A2. Liver tissue blocks were prepared from three different mice and used for 3D analysis. Representative images acquired from hilum and peripheral tissue are shown in this figure. Boxes in b and f are enlarged in c-e and g-i, respectively. Scale bars: 200 µm in Aa and Bb,f; 50 µm in Ab,c and Be,i. CV, central vein.

tubulin (TUBB3) were found next to a large IHBD positive for osteopontin (OPN) and a HA positive for CD31 (Fig.1Ab, closed arrowheads), whereas fine nerve fibers were found around the PV (Fig.1Ab, open arrowheads). IHBDs in the peripheral Glisson's sheath were clearly associated with TUBB3$^+$ nerve fibers (Fig.1Ac, open arrowheads). To further characterize the spatial localization of nerve fibers, we performed whole-mount immunostaining of adult liver tissue blocks and 3D imaging using a confocal laser-scanning microscope (Fig. 1B). Around a large PV, thick nerve fibers ran along a large IHBD tubule (Fig. 1Bc,e, closed arrowheads), whereas fine nerve fibers were observed along the PV (Fig. 1Bc,e, open arrowheads). As expected from 2D analyses, IHBDs were associated with nerve fibers even in the periphery of the liver (Fig. 1Bf-i). However, the nerve fibers did not extend into the parenchymal region. Taken together, nerve fibers form the network in the periportal tissue, but not parenchymal tissue, of adult mouse liver, indicating that the intrahepatic nerve network of mice is similar to that of rats.

Establishment of the nerve network during liver organogenesis

To understand how the intrahepatic nerve network is established during organogenesis, we first examined expression of TUBB3 on embryonic day 17.5 (E17.5) liver (Fig. 2A). TUBB3$^+$ fibers were observed alongside extrahepatic bile ducts (EHBDs) (Fig. 2Ab, closed arrowheads), whereas they were not detected around IHBDs (Fig. 2Ac). This result indicates that nerve fibers have not extended into intrahepatic tissue by E17.5. We also examined liver tissue at postnatal day 1 (P1) and could not find TUBB3$^+$ fibers inside the liver (data not shown). Next, we examined TUBB3 expression in liver 1 week after birth (1W) (Fig. 2B). At this stage, TUBB3$^+$ fibers were located around IHBDs (Fig. 2Bb, closed arrowheads), HAs (Fig. 2Bc, closed arrowheads) and PVs (Fig. 2Bc, open arrowheads). However, TUBB3$^+$ fibers were absent from the periphery of the liver, even though an IHBD network containing large ducts and small ductules was already established in this area (Fig. 2Bd). To further examine such heterogeneous tissue structures

Development (2018) 145, dev159095. doi:10.1242/dev.159095

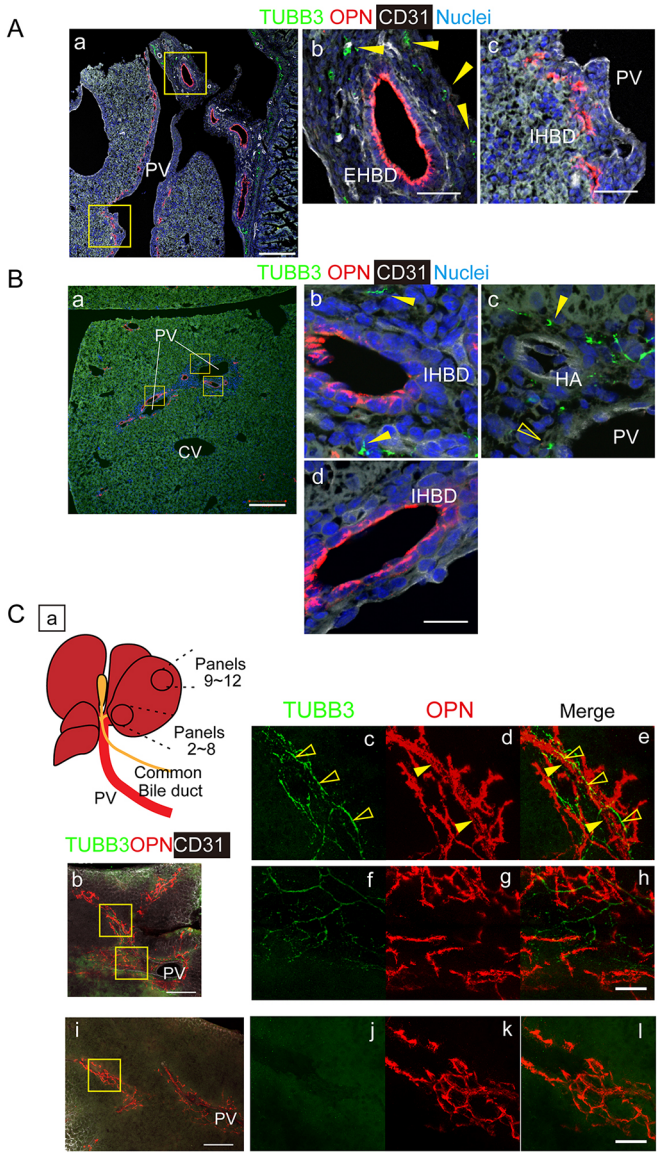

Fig. 2. Development of the intrahepatic nerve network. (A) Nerve fibers do not enter the intrahepatic tissue at E17.5. Nerve fibers exist next to EHBDs (b, arrowheads), but not IHBDs (c). At this stage, large bile duct tubules have not developed. An E17.5 liver section was stained with anti-TUBB3, anti-OPN and anti-CD31 antibodies. Sections prepared from three mice were used for immunostaining and representative data are shown in this figure. Boxes in panel a are enlarged in b,c. (B) Nerve fibers are associated with IHBDs near the liver hilum at 1W. Nerve fibers are observed near the IHBDs (b, closed arrowheads), HA and PV (b, closed and open arrowheads, respectively). However, a large IHBD near the periphery is not associated with nerve fibers at this stage (d). Neonatal (1W) liver sections were stained with anti-TUBB3, anti-OPN and anti-CD31 antibodies. Sections prepared from three mice were used for immunostaining and representative data are shown in this figure. (C) IHBDs are associated with nerve fibers in the hilum, but not the periphery, of the liver at 1W. IHBDs and the nerve network were examined near the hilum and in the peripheral region (a). Nerve fibers are evident near the liver hilum (b-h). A nerve fiber (c,e, open arrowhead) runs along a large IHBD tubule (d,e, closed arrowheads). Nerve fibers that are not parallel to IHBDs are evident and surround the PV (c-h). However, nerve fibers have not extended to the periphery of the liver (i-l). Neonatal liver tissue blocks were incubated with anti-TUBB3, anti-OPN and anti-CD31 antibodies and cleared in SCALEVIEW-A2. Liver tissue blocks were prepared from three different mice and used for 3D analysis. Representative images acquired on a tissue block are shown in this figure. Scale bars: 200 µm in Aa, Ba and Cb,i; 50 µm in Ab,c and Ch,l; 20 µm in Bb-d.

in neonatal liver, we performed 3D imaging using 1W liver tissue blocks and analyzed the nerve network in the liver hilum and the peripheral region (Fig. 2Ca). Consistent with the 2D analyses, a nerve network was observed around the PVs near the liver hilum (Fig. 2Cb-h). A nerve fiber (Fig. 2Cc,e, open arrowheads) ran along a large IHBD tubule (Fig. 2Cd,e, closed arrowheads). However, compared with the adult nerve network, the nerve fibers were relatively fine and homogenous. Notably, as expected from 2D analyses, TUBB3$^+$ nerve fibers were not observed around the PVs in the liver periphery at 1W (Fig. 2Ci-l). We also examined TUBB3$^+$ nerve fibers in 2W and 3W liver. TUBB3$^+$ nerve fibers were found in the periphery at 3W (Fig. S1), indicating that hepatic nerve fibers gradually extend from the liver hilum to the periphery by 3W after birth.

NGF derived from IHBDs is correlated with the extension of nerve fibers

The close association between IHBDs and nerve fibers suggested that BECs secrete factors inducing the extension of nerve fibers. Neurotrophic factors have been previously correlated with the extension of nerve fibers along blood vessels and epithelial tissue structures (Lu and Werb, 2008). For example, glial cell line-derived neurotrophic factor (GDNF) is strongly expressed in the gut mesenchyme, which is involved in the innervation of gut tissue (Peters et al., 1998).

To investigate this possibility, we used quantitative PCR to examine the expression of *Bdnf*, *Gdnf*, *Ngf*, *Nt3* (*Ntf3*) and *Nt5* (*Ntf5*) in neonatal and adult BECs (Fig. S2). *Ngf*, *Nt3* and *Nt5* were expressed in BECs, whereas *Bdnf* and *Gdnf* were not detected. Relative to the expression levels of these neurotrophic factors in embryonic brain and neonatal kidney, which served as a control in this experiment, *Ngf* was more strongly expressed in BECs than were *Nt3* and *Nt5*. In addition, TRKA (Ntrk1), a receptor for NGF, was detected in intrahepatic nerve fibers (Fig. S3). We then examined *Ngf* expression in hepatocytes, CD31$^+$ ECs, EpCAM$^+$ BECs and Thy1$^+$ MCs isolated from 1W and adult livers to assess whether *Ngf* is exclusively expressed in BECs. We found that *Ngf* was expressed not only in EpCAM$^+$ BECs, but also in Thy1$^+$ MCs (Fig. 3A), suggesting that IHBDs composed of BECs and Thy1$^+$ MCs supply NGF for the extension of nerve fibers (Fig. 3B). The lower expression of *Ngf* in hepatocytes was consistent with the observation that nerve fibers were not distributed in the parenchymal region (Fig. 3A). Thus, *Ngf* expression in adult CD31$^+$ cells might be correlated with the maintenance of TUBB3$^+$ nerve fibers around PVs and HAs.

To correlate *Ngf* expression in IHBDs with establishment of the nerve network, we examined the expression of *Ngf* in BECs and Thy1$^+$ MCs during development (Fig. 3C). *Ngf* was significantly upregulated between P5 and 1W in both BECs and Thy1$^+$ MCs. We also examined NGF expression by immunofluorescence chemistry. In 1W liver tissue, NGF was detected in IHBDs, including BECs and Thy1$^+$ MCs with or without associated nerve fibers (Fig. S4Aa-f versus Fig. S4Ag-l). By contrast, NGF was expressed at extremely low levels in P2 liver (Fig. S4Ba-l).

Based on these results, we propose a model for the development of the intrahepatic nerve network in mice (Fig. 3D). In a fetus, nerve fibers are excluded from intrahepatic tissue, and the fibers begin entering liver tissue only after birth. At 1W, NGF is significantly expressed in IHBDs and nerve fibers are extended, but do not reach the periphery. By 3W, nerve fibers cover the entire liver.

Development (2018) 145, dev159095. doi:10.1242/dev.159095

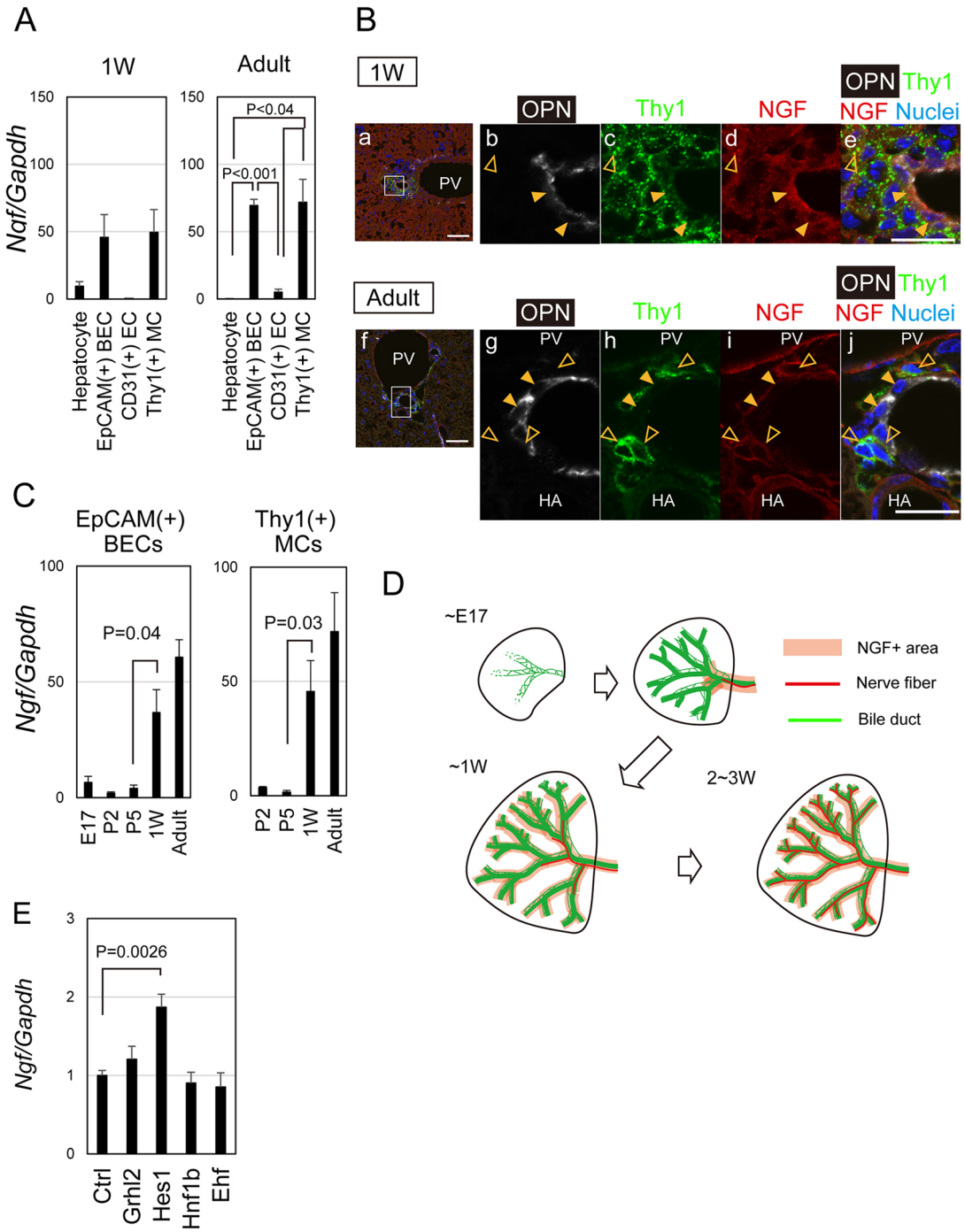

Fig. 3. BECs and Thy1$^+$ MCs express NGF. (A) *Ngf* is expressed in BECs and periportal MCs. *Ngf* is detected in EpCAM$^+$ BECs and periportal Thy1$^+$ MCs both at 1W and in adults, but weakly and minimally expressed in ECs and hepatocytes, respectively. Hepatocytes, EpCAM$^+$ BECs, CD31$^+$ ECs and Thy1$^+$ MCs were isolated from 1W and adult (8-12W) livers. BECs, ECs and MCs were isolated from CD45$^-$ fractions. Cell isolation was repeated three times at 1W, twice at 8W and once at 12W. (B) Thy1$^+$ MCs surround BECs in neonatal and adult livers. Thy1$^+$ cells surround OPN$^+$ BECs in neonatal and adult livers. NGF$^+$ BECs (closed arrowheads) and MCs (open arrowheads) exist in neonatal and adult livers. In adult liver, ECs of the PV and HA are also positive for NGF. (C) *Ngf* expression in BECs and MCs is upregulated during liver development. *Ngf* expression increases in BECs and MCs during development. Expression is significantly upregulated between P5 and 1W when nerve fibers are entering the liver tissue. To examine *Ngf* expression, we used 1W kidneys as a control. Relative *Ngf* expression levels are shown in the graph. Cell isolation was repeated three times at E17, P2 and P5, and five times at 1W and in adults. Samples at the 1W and adult stages included EpCAM$^+$ BECs and Thy1$^+$ MCs used in A. (D) Model for formation of the intrahepatic nerve network during development. In fetal liver, TUBB3$^+$ nerve fibers are observed around EHBDs but are excluded from intrahepatic tissue. In neonatal liver, TUBB3$^+$ nerve fibers are evident near the hilum but not in the periphery. By 3 weeks after birth, the nerve network covers the entire liver tissue. Expression of NGF gradually increases in IHBDs during postnatal development. NGF expression in IHBDs precedes the formation of the intrahepatic nerve network. (E) *Ngf* is upregulated by Hes1, but not by Ehf, Hnf1β or Grhl2. HPPL, a liver progenitor cell line, was infected with retrovirus vectors containing cDNA of Ehf, Grhl2, Hes1 or Hnf1β. The expression levels of *Ngf* relative to control cells are shown in the graph. Retrovirus infection was repeated three times, independently. Bars in A,C and E represent s.e.m. Two-tailed Student's *t*-tests were performed for data in A,C and E using Microsoft Excel. Scale bars: 50 µm in Ba,f; 20 µm in e,j.

Development (2018) 145, dev159095. doi:10.1242/dev.159095

Regulation of NGF expression

Our results suggest that the expression of *Ngf* in IHBDs is upregulated in correlation with their tubular morphogenesis. Although transcriptional regulation in Thy1$^+$ MCs remains unknown, several transcription factors are upregulated during the lineage commitment of hepatoblasts (fetal liver stem/progenitor cells) to BECs and the subsequent tubular morphogenesis. Those transcription factors include ets homologous factor (Ehf), the hairy enhancer of slit 1 (Hes family bHLH transcription factor 1; Hes1), hepatocyte nuclear factor 1β, (Hnf1β) (Fig. S5A) and grainyhead like 2 (Grhl2) (Senga et al., 2012). To identify the upstream mechanisms regulating *Ngf* expression in BECs, we overexpressed BEC-specific transcription factors in a liver progenitor cell line, HPPL (Tanimizu et al., 2004). Of these factors, Hes1 significantly upregulated *Ngf* in HPPL (Fig. 3E). Hes1 is a target of the Notch signaling pathway, a major signal regulating IHBD development; therefore, Hes1 expression is upregulated at the point at which hepatoblasts are committed to become BECs. However, Hes1 expression was also significantly increased from P5 to 1W (Fig. S5B), the same period during which *Ngf* was upregulated in EpCAM$^+$ BECs (Fig. 3C). Furthermore, the 5′-untranslated region of the mouse and human genes encoding NGF contains two conserved N-box sequences (Fig. S5C). These data suggest that Hes1 is involved in the transcriptional regulation of *Ngf* in BECs.

Ectopic expression of NGF is sufficient for modulating the intrahepatic nerve network

To further confirm whether NGF is a crucial factor for the extension of nerve fibers in liver, we induced the expression of NGF in mature hepatocytes (MHs) by administering via a hydrodynamic tail vein injection (HTVi) an expression vector containing the cDNA of NGF (Fig. 4A). As shown in Fig. S6, ectopic gene expression was predominantly detected in pericentral hepatocytes following HTVi with a pLIVE vector. At 1W after HTVi, nerve fibers were increased around the PVs and observed in the parenchymal region (Fig. 4Bb, arrowheads), where they are normally excluded (Fig. 4Ba). At 4W after HTVi, TUBB$^+$ nerve fibers further extended through the intercellular spaces among HNF4α$^+$ hepatocytes (Fig. 4Cb,c) and occasionally reached the central vein (Fig. 4Cd,e). To show the gradual extension of nerve fibers by ectopic NGF, we defined three areas in the liver lobule along the PV–CV axis and quantified the intensity of TUBB3 in those areas. As shown in Fig. S6B,C, TUBB3$^+$ fibers were restricted in the portal triad in control animals, whereas they occurred in the periportal area at 1W. Furthermore, TUBB3$^+$ fibers in the parenchyma increased between 1W and 4W after HTVi other than the periportal area. Therefore, ectopic NGF induces the extension of nerve fibers from the periportal area toward the pericentral area. These results indicate that the intrahepatic nerve network can be rearranged by the ectopic expression of NGF.

Regeneration of the nerve network after bile duct injury

Lastly, we examined whether the nerve network can be regenerated after liver injury and, if so, how the regeneration progresses. Given that the nerve network is strongly associated with IHBDs, we selected a bile duct injury model induced by 4,4-diaminodiphenylmethane (DAPM). First, we examined the destruction and regeneration of the IHBD network in the entire liver tissue by a retrograde injection of carbon ink into the biliary system at the junction between the common bile duct and the duodenum (Kaneko et al., 2015; Tanimizu et al., 2016). As we previously reported, a continuous luminal network consisting of large ducts and small ductules was visualized (Fig. 5Aa,b). At 2 days

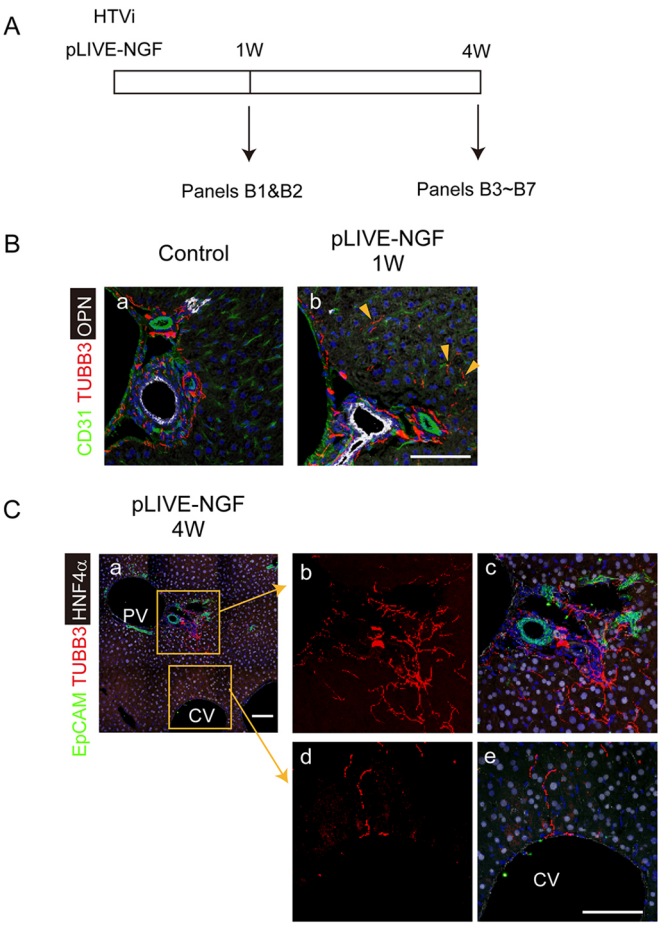

Fig. 4. Ectopic expression of NGF induces extension of nerve fibers. (A) Examination of the effect of NGF expression in mature hepatocytes. A plasmid encoding NGF (pLIVE-NGF) was introduced into MHs by HTVi. At 1W and 4W after HTVi, the intrahepatic nerve network was examined by immunohistochemistry. HTVi was performed on six mice. Three mice each were examined for expansion of nerve fibers at 1W and 4 W. (B) TUBB3$^+$ nerve fibers increase around the PVs at 1W after HTVi. TUBB3$^+$ nerve fibers are abundant around the PV and observed in the parenchymal region (b, arrowheads) in the liver administrated with pLIVE-NGF, whereas their localization is limited next to the PV in the control (a). Liver sections were stained with anti-CD31, anti-TUBB3 and anti-OPN antibodies, and nuclei were counterstained with Hoechst 33342. (C) TUBB3$^+$ nerve fibers are further extended and reach the CV area. TUBB3$^+$ nerve fibers are further extended in the parenchymal region through the intercellular spaces of HNF4α$^+$ MHs and occasionally reach the central vein (CV) at 4W after HTVi. Liver sections were stained with anti-EpCAM, anti-TUBB3 and anti-HNF4α antibodies, and nuclei were counterstained with Hoechst 33342. The two boxes in panel a are enlarged in b,c and d,e. Scale bars: 100 µm in B,C.

after DAPM injection, carbon ink was observed leaking from IHBDs. This indicated that the continuity of the luminal network had been disrupted (Fig. 5Ac,d). The loss of small ductules and dilation of large IHBDs was confirmed by immunohistochemical analysis (data not shown). By 12 days after DAPM administration, a continuous luminal network had been regenerated (Fig. 5Ae,f). Next, alternation of the intrahepatic nerve network was examined by immunohistochemical analyses. EpCAM$^+$ bile ducts were associated with TUBB3$^+$ nerve fibers in normal liver (Fig. 5Ba,b). Although EpCAM$^+$ bile ducts were still present, nerve fibers were frequently absent from the PV area in the periphery at days 2 and 4 (Fig. 5Bc-f). By day 12, IHBDs had been regenerated and were mostly associated with nerve fibers (Fig. 5Bg,h). To acquire

Development (2018) 145, dev159095. doi:10.1242/dev.159095

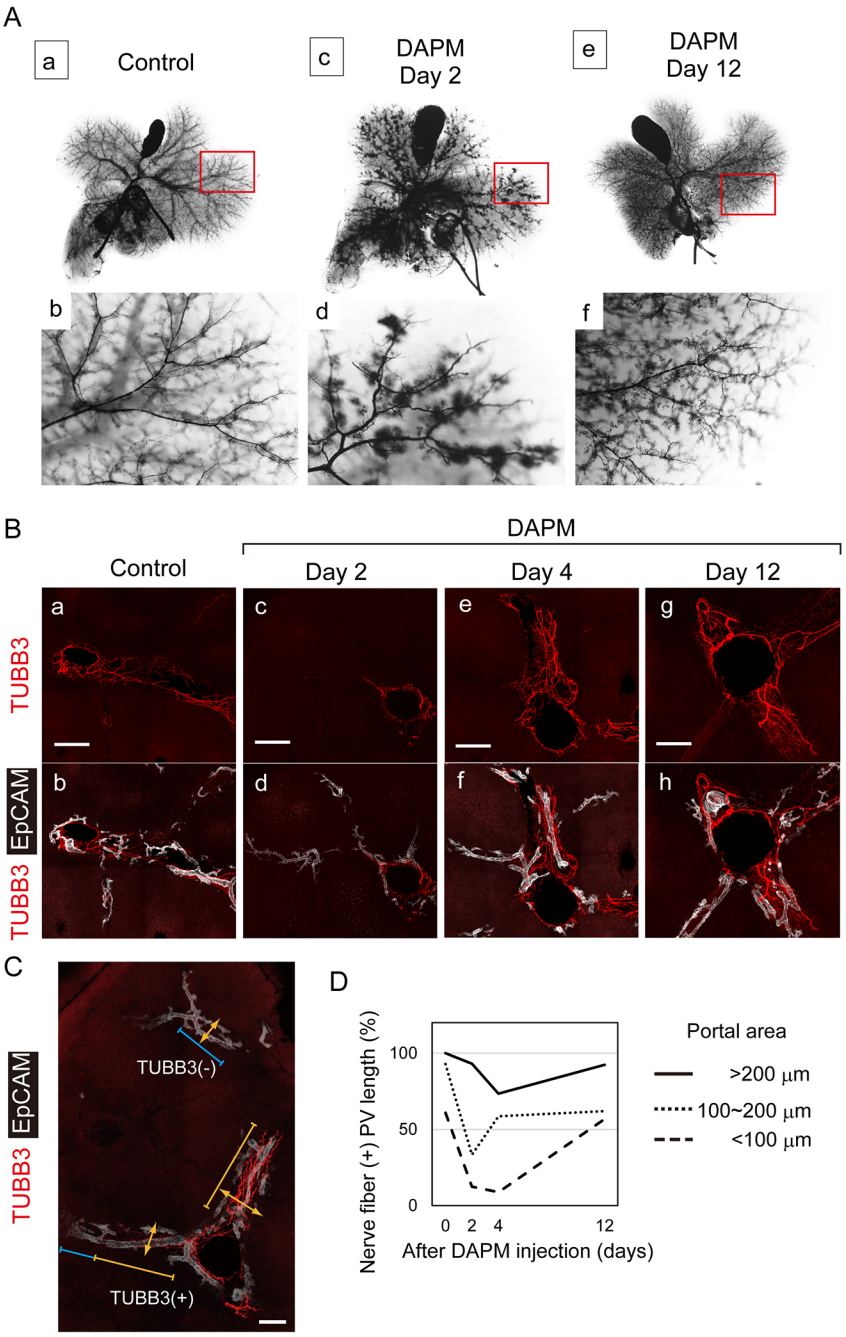

Fig. 5. Regeneration of the nerve network in liver tissue after acute biliary injury. (A) Destruction and regeneration of the luminal network of IHBDs after DAPM administration. The continuous luminal network of IHBDs consists of large ducts and small mesh-like ductules in a normal liver (a,b). At 48 h after DAPM administration, carbon ink is observed to leak from IHBDs throughout the liver tissue, indicating that the continuity of the luminal network has been destroyed (c,d). At this stage, the luminal space of large ducts appears dilated, whereas the fine mesh-like luminal network cannot be clearly visualized. At 12 days, the continuous luminal network containing small ductules is regenerated (e,f). Ink injection was repeated three times at each time point. (B) Effect of DAPM administration on the nerve network. EpCAM$^+$ bile ducts are associated with TUBB3$^+$ nerve fibers in normal liver (a,b). At 48 h after DAPM administration, EpCAM$^+$ dilated bile ducts without TUBB3$^+$ fibers are evident (c,d). At 12 days, the association of TUBB3$^+$ nerve fibers with EpCAM$^+$ bile ducts has mostly recovered. Thick (300 µm) liver sections were incubated with anti-EpCAM and anti-TUBB3 antibodies. Optical sections acquired on a confocal laser scanning microscope were reconstituted and the projection images are shown in a-h. Thick sections were prepared from three or four mice at each time point, and images were acquired from four different areas per mouse. (C) Quantification of nerve regeneration after DAPM injury. The diameters of the PV areas surrounded by IHBDs (arrows), lengths of the PV areas associated with both IHBDs and nerve fibers (red lines), and lengths of PV areas associated only with IHBDs (blue lines) were measured in Image J. A thick liver section prepared 4 days after DAPM administration was incubated with anti-TUBB3 (red) and anti-EpCAM (white) antibodies. (D) Quantitative analysis of the regeneration of the nerve network. Nerve fibers shrink from the periphery when the IHBDs are destroyed either 2 or 4 days after DAPM administration. Nerve fibers are mostly reconstructed by 12 days. PV areas were divided into three groups according to the diameter of the region surrounded by IHBDs. Wide (>200 µm) and narrow (<100 µm) areas were assumed to represent hilum and peripheral tissues, respectively. Scale bars: 250 µm in B and 100 µm in C.

quantitative data on the destruction and regeneration of nerve fibers, we quantified the association between nerve fibers and IHBDs at different locations within liver tissue. Overall, the PV area was wide in the hilum and narrow in the periphery. Thus, by measuring the diameters of PV areas, we could assume their locations. Using 3D-reconstructed images, we measured the diameters of PV areas surrounded by IHBDs in Image J (Fig. 5C, yellow arrows) and then divided these areas into three groups based on these measurements. Next, we measured the lengths of PV areas associated with both IHBDs and nerve fibers (Fig. 5C, yellow lines) and those only associated with IHBDs (Fig. 5C, blue lines). The results showed that the association between nerve fibers and IHBDs was significantly disrupted in most liver tissue, except near the wide PV areas (diameters >200 µm), at days 2 and 4 after DAPM injection (Fig. 5D). By 12 days after DAPM administration, IHBDs were regenerated and were mostly associated with nerve fibers.

After DAPM injury, *Ngf*, but not *Nt3* or *Nt5*, was transiently increased at day 2 (Fig. 6A). As in normal liver, BECs and Thy1$^+$ MCs mainly expressed *Ngf* (Fig. 6B), which is consistent with nerve fibers being reconstructed along IHBDs. The expression level of *Ngf* in BECs and MCs at day 2 was comparable to that in controls. Given that IHBDs include many Ki67$^+$ cells, expansion of BECs and Thy1$^+$ cells might be correlated with the transient upregulation of *Ngf* within liver tissue at day 2. In the regenerating liver, CD31$^+$ ECs also expressed *Ngf*, which might also increase the overall *Ngf* expression in liver tissue.

To evaluate the role of neurotrophic factors, such as NGF, in the reorganization of the nerve network, Trk inhibitors were used to inhibit signals during regeneration after DAPM injury. Given that

Development (2018) 145, dev159095. doi:10.1242/dev.159095

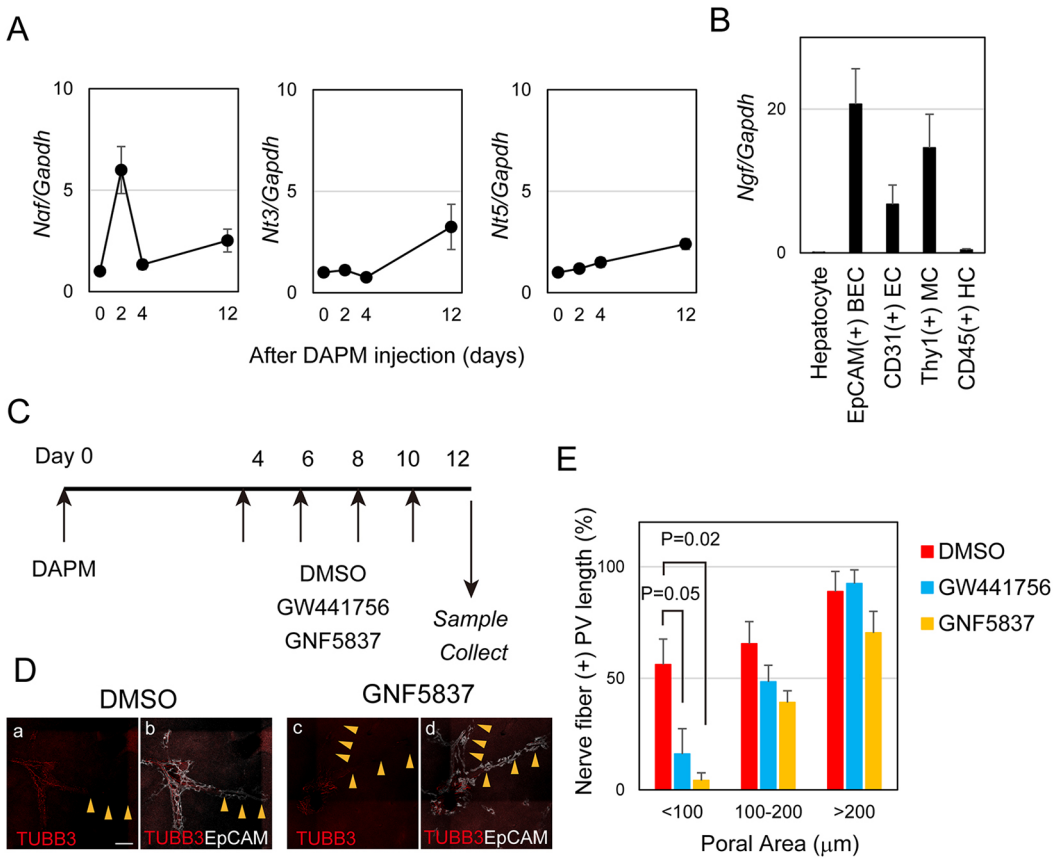

Fig. 6. Inhibition of NGF signal attenuates reinnervation of liver tissue. (A) Expression of neurotrophic factors during recovery from DAPM injury. Expression of *Ngf* transiently increases at 2 days after DAMP administration and returns to normal levels at 4 days. *Nt3* and *Nt5* are slightly upregulated at day 12. Three mice were used to examine *Ngf*, *Nt3* and *Nt5* at each time point. (B) Expression of *Ngf* in BECs, Thy1$^+$ MCs and ECs. *Ngf* is mainly expressed in EpCAM$^+$ BECs and Thy1$^+$ MCs at day 2. ECs also express *Ngf* at this time point. Relative expression levels of *Ngf* compared with neonatal (1W) kidney, which is used as a control, are shown in the graphs. Cell isolation from liver at day 2 of DAPM injury was repeated three times. (C) Experimental design for NGF inhibition during regeneration. DAPM (50 mg/kg) is intraperitoneally injected into mice to induce biliary injury. From 4 days after DAPM injection, mice are administered 8 mg/kg GW551746 or GNF5837 every 2 days. At day 12, liver tissue is collected and fixed for the following experiments. (D) Reorganization of the nerve network is attenuated by suppression of Trk receptors. Reinnervation appears attenuated in narrow portal areas in mice administered GNF5837 (c,d, arrowheads) compared with control mice administered DMSO (a,b, arrowheads). By contrast, the wide portal areas associated with large IHBDs are reinnervated both in controls and mice administered GNF5837. (E) Quantitative analysis of the effect of Trk inhibitors on reorganization of the nerve network. Reinnervation in narrow portal areas is significantly attenuated by GW441756 and GNF8537. Three mice were administered DMSO and GNF5547, whereas four mice were administered GW441756. Four thick sections (300 µm) were prepared from each mouse. One or two areas were selected in each section for the acquisition of images of 120 µm thickness. Bars represent s.e.m.. Two-tailed student's *t*-tests were performed using Microsoft Excel. Scale bar: 200 µm in D.

the nerve network is reestablished between days 4 and 12 (Fig. 5D), we intraperitoneally injected GW441756 or GNF5837 into mice every 2 days, starting from day 4 after DAPM injection, and then examined the liver tissue at day 12 (Fig. 6C). Reorganization of the nerve network around IHBDs appeared to be attenuated with GNF5837 (Fig. 6D). Quantitative analysis of the ratio of TUBB3$^+$ PV areas over the total PV areas showed that regeneration of nerve fibers in narrow PV areas was attenuated by either GW441756 or GNF5837 (Fig. 6E).

These results suggest that NGF secreted by IHBDs is necessary to induce the reorganization of the liver nerve network during regeneration. Thus, we assume that disruption of IHBDs causes the regression of nerve fibers and that the regeneration of the nerve network follows the regeneration of IHBDs in liver (Fig. S7).

DISCUSSION

This work demonstrated the developmental and regenerative processes of the mouse intrahepatic nerve network. Formation of the nerve network followed tubular morphogenesis of IHBDs during development. Upregulation of *Ngf*, which is partly regulated by HES1, in IHBDs preceded the extension of nerve fibers within liver tissue. NGF derived from BECs and Thy1$^+$ MCs, which are epithelial and mesenchymal components of IHBDs, respectively, was required for the regeneration of nerve fibers. Ectopic expression of NGF in hepatocytes induced the extension of nerve fibers into the parenchymal region, from where they are normally excluded. Therefore, IHBDs supply NGF and guide the formation of the nerve network.

NGF is a major neurotrophic factor. The requirement for NGF for sympathetic innervation was examined using *Ngf* knockout mice in a *Bax*$^{-/-}$ background, because NGF was expected to be necessary for both the extension of nerve fibers and their survival (Glebova and Ginty, 2004). In *Ngf*$^{-/-}$ *Bax*$^{-/-}$ mice, sympathetic innervation was deficient in the heart and greatly reduced in several organs, including the lung, pancreas and spleen. Innervation of the liver was also greatly reduced at both E16.5 and P0.5 in *Ngf*$^{-/-}$ *Bax*$^{-/-}$ mice. In normal mice, although common bile ducts and the gallbladder are already innervated at the fetal stage (Fig. 2), nerve fibers only started entering the intrahepatic tissue after birth. Our data newly

Development (2018) 145, dev159095. doi:10.1242/dev.159095

demonstrate that NGF expression in IHBDs precedes the formation of the intrahepatic nerve network during postnatal development.

In addition to the developmental process, we examined the reorganization of the nerve network during regeneration of IHBDs after DAPM administration. Given that the selective inhibition of TRKA (a receptor for NGF) with GW441756 significantly attenuated extension of nerve fibers after DAPM injury, NGF derived from IHBDs is required for the regeneration of the nerve network. GNF5837, which inhibits TRKA, B and C, attenuated nerve regeneration more severely than did GW441756, suggesting that NT3 and NT5 function redundantly for regeneration in the absence of a NGF-TRKA signal, although their expression is much weaker than that of NGF. Taken together, our findings indicate that regeneration of IHBDs precedes regeneration of the nerve network and that the IHBDs supply NGF, which induces the reestablishment of the intrahepatic nerve network.

The physiological importance of the hepatic nerve system has been investigated using experimental models in which hepatic nerves are dissociated from the central nervous system by subdiaphragmatic vagotomy (Jensen et al., 2013) or by the systemic infusion of chemicals stimulating or inhibiting autonomic neurons (Oben and Diehl, 2004). In addition, the cellular characteristics of hepatic stellate cells (HSCs), which have crucial roles in liver fibrosis, have been correlated with functions of neurotransmitters (Oben and Diehl, 2004). It was demonstrated that HSCs express catecholamine biosynthetic enzymes and receptors, and that norepinephrine, a catecholamine, promotes HSC proliferation. Furthermore, dopamine β-hydroxylase-deficient ($Dbh^{-/-}$) mice, which cannot make norepinephrine, were resistant to injury-related liver fibrogenesis, and $Dbh^{-/-}$ HSCs did not proliferate without exogenous norepinephrine. However, it remains unclear how the intrahepatic nerve network is correlated with HSC activation and fibrogenesis.

It has been reported that periportal tissues are innervated with both sympathetic and parasympathetic nerves in mammals (Jensen et al., 2013). In addition, sympathetic nerves enter the parenchymal tissue in dogs, guinea pigs and humans, but not in rats (Ueno et al., 2004). We examined the expression of tyrosine hydroxylase (Th) and vesicular acetylcholine transporter [VAChT; solute carrier family 18 (vesicular monoamine), member 3 (Slc18a3)] to determine whether nerve fibers in the mouse liver are sympathetic or parasympathetic. TUBB3^{+} nerves were mostly Th^{+}, whereas VAChT^{+} fibers were only observed near the large IHBDs (Fig. S8). These results suggest that liver tissue is thoroughly innervated with sympathetic nerves, whereas parasympathetic nerves exist mainly in the hilum region. Hepatic parasympathetic nerves are derived from vagus nerves and have crucial roles in regulating blood flow and metabolic reactions in the liver. To understand the role of the autonomic nerve system in the liver, it will be important to further characterize the localization of sympathetic and parasympathetic nerves within liver tissue.

This work also demonstrated the development and regeneration of neuro-epithelial wiring in the liver. In both processes, IHBDs guide the formation of the nerve network, and NGF derived from BECs and MCs likely has a crucial role in the extension of nerve fibers. We demonstrated that the nerve network can be modulated by introducing NGF to MHs: nerve fibers extended into the parenchymal region, which is also observed in human liver tissue. Given the various acute and chronic liver injury models available, as well as the availability of experimental methods reducing or increasing nerve fibers and stimulating or suppressing autonomic nerves, the liver serves as a good experimental model for understanding the molecular mechanisms governing neuro-epithelial wiring during development, chronic injury and regeneration.

MATERIALS AND METHODS

Mice

Pregnant female C57BL6 mice were purchased from Sankyo Labo Service Corporation (Tokyo, Japan) to acquire embryos and newborn mice for experiments. Adult male and female mice (8-12W) were also purchased. Female mice were used for HTVi. For other experiments, adult male mice were used. All animal experiments were approved by the Sapporo Medical University Institutional Animal Care and Use Committee and were conducted according to institutional guidelines for ethical animal use.

Immunostaining and confocal imaging

Neonatal and adult liver tissues were fixed in PBS containing 4% paraformaldehyde at 4°C. After being embedded in OCT compound, 0.7 µm frozen sections were prepared on a cryostat (Leica). Fixed liver tissue was also used for whole-mount immunostaining, as previously reported (Tanimizu et al., 2016). Tissue blocks were cleared in SCALEVIEW-A2 (Olympus). The primary antibodies used for immunostaining are listed in Table S1. Images were acquired using a Zeiss LSM780 confocal laser scanning microscope (Carl Zeiss).

Cell isolation and sorting

Embryonic and neonatal livers were digested by Librase TM (Roche). Normal and DAPM-injured adult livers were digested with a two-step collagenase perfusion method, as previously reported (Tanimizu et al., 2014). Briefly, hepatocytes were collected by centrifugation at 50 ***g*** for 1 min. The tissue remnant after collagenase perfusion was further digested by collagenase and hyaluronidase, and the cell suspension was then centrifuged at 350 ***g*** for 4 min to collect nonparenchymal cells containing BECs, ECs and MCs. Nonspecific binding of antibodies to nonparenchymal cells was blocked by an antibody against the Fcγ receptor (anti-CD16/CD32 antibody, BD Biosciences). Cells were labeled with Alexa Fluor 488-conjugated anti-Thy1 (Biolegend), APC-conjugated anti-EpCAM (Biolegend), APC-Cy7-conjugated anti-CD45 (BD Biosciences), PE-Cy7-conjugated anti-CD31 (Biolegend) antibodies and propidium iodide (Sigma-Aldrich). Cell isolation was performed using a FACSAria II flow cytometer (BD Biosciences).

PCR

Total RNA was extracted from liver tissue and cultured cells and used for cDNA synthesis. Primer sequences used for quantitative PCR with SYBR Green Premix Ex Taq II (Tli RNase H Plus; Takara Bio) are listed in Table S2. To examine the expression of *Hes1*, *Hnf1b* and *Hprt*, we used Premix Ex Taq (Probe qPCR; Takara Bio) and TaqMan probes (Life Technologies).

Cell culture and transfection

HPPL is a bipotential liver progenitor cell line that was established from E14.5 mouse hepatoblasts. HPPLs were transfected by retrovirus vectors pMXs-Neo containing Grhl2, Hes1, Hnf1β or Ehf, and treated with 0.1 mg/ml G418. PCR cloning for Ehf, Grhl2 and Hnf1β was as previously reported (Senga et al., 2012). The mouse Hes1 coding sequence, with an added Myc tag at the N-terminus, was amplified by PCR with the primers shown in Table S2.

Hydrodynamic tail vein injection

The mouse NGF coding sequence was amplified by PCR and inserted into a pLIVE expression vector (Mirus Bio). Next, 20 µg plasmid DNA was suspended in *Trans*IT-EE hydrodynamic delivery solution (Mirus Bio) equal to 10% of body weight. The plasmid solution was injected into mice via the tail vein within 5-8 s, as previously reported (Herweijer et al., 2001).

DAPM injury and visualization of the luminal network of IHBDs

Mice (8-10W) were administered DAPM by peritoneal injection and then sacrificed at day 2, 4 or 12 to examine their liver tissue. Carbon ink injection

Development (2018) 145, dev159095. doi:10.1242/dev.159095

was performed as previously reported (Kaneko et al., 2015). Briefly, a glass capillary was inserted into the junction between the common bile duct and the duodenum and ink was retrogradely injected. Livers were dehydrated in ethanol and then cleared in a solution containing 2 volumes of benzyl alcohol and 1 volume of benzoyl benzoate.

Inhibition of the signals activated by neurotrophic factors

GW441756 (Alomone Labs) and GNF5837 (AdooQ Bioscience) were dissolved in DMSO to make 50 mM stock solutions. Before being injected, Trk inhibitors were diluted at a 1:10 ratio in DMSO. Then, 100 µl of the diluted solution was intraperitoneally injected into each mouse. For quantitative analysis, thick sections (300 µm) were prepared and used for immunostaining and clearing with triethanol amine. Images acquired from thick sections of DAPM injured liver were used for quantitative analysis. The width of PV areas and the length of areas with or without TUBB3^{+} nerves were measured using ImageJ.

Acknowledgements

We thank Ms Yumiko Tsukamoto and Ms Minako Kuwano for technical assistance. We also thank Enago (Japan) for the English language review.

Competing interests

The authors declare no competing or financial interests.

Author contributions

Conceptualization: N.T.; Methodology: N.T.; Validation: N.T., N.I.; Formal analysis: N.T.; Investigation: N.T.; Resources: N.T.; Data curation: N.T.; Writing - original draft: N.T.; Writing - review & editing: T.M.; Funding acquisition: N.T.

Funding

This work is supported by Japan Society for the Promotion of Science; by Grants-in-Aid for Scientific Research (C) (25460271 and 16K08716 to N.T.); by Grants-in-Aid for Scientific Research on Innovative Areas 'Stem Cell Aging and Disease' (17H05653 to N.T.); Grants-in-Aid for Scientific Research (B) (21390365 and 24390304 to T.M.); and by Grants-in-Aid for Exploratory Research (24659591, 26670584 and 17K19703 to T.M.).

Supplementary information

Supplementary information available online at
http://dev.biologists.org/lookup/doi/10.1242/dev.159095.supplemental

References

Alvaro, D., Alpini, G., Jezequel, A. M., Bassotti, C., Francia, C., Fraioli, F., Romeo, R., Marucci, L., Le Sage, G., Glaser, S. S. et al. (1997). Role and mechanisms of action of acetylcholine in the regulation of rat cholangiocyte secretory functions. *J. Clin. Invest.* **100**, 1349-1362.

Barja, F. and Mathison, R. (1984). Sensory innervation of the rat portal vein and the hepatic artery. *J. Auton. Nerv. Syst.* **10**, 117-125.

Brunet, I., Gordon, E., Han, J., Cristofaro, B., Broqueres-You, D., Liu, C., Bouvrée, K., Zhang, J., del Toro, R., Mathivet, T. et al. (2014). Netrin-1 controls sympathetic arterial innervation. *J. Clin. Invest.* **124**, 3230-3240.

Carmeliet, P. and Tessier-Lavigne, M. (2005). Common mechanisms of nerve and blood vessel wiring. *Nature* **436**, 193-200.

Cox, J. E., Kelm, G. R., Meller, S. T., Spraggins, D. S. and Randich, A. (2004). Truncal and hepatic vagotomy reduce suppression of feeding by jejunal lipid infusions. *Physiol. Behav.* **81**, 29-36.

Fukuda, Y., Imoto, M., Koyama, Y., Miyazawa, Y. and Hayakawa, T. (1996). Demonstration of noradrenaline-immunoreactive nerve fibers in the liver. *J. Int. Med. Res.* **24**, 466-472.

Glebova, N. O. and Ginty, D. D. (2004). Heterogeneous requirement of NGF for sympathetic target innervation in vivo. *J. Neurosci.* **24**, 743-751.

Herweijer, H., Zhang, G., Subbotin, V. M., Budker, V., Williams, P. and Wolff, J. A. (2001). Time course of gene expression after plasmid DNA gene transfer to the liver. *J. Gene. Med.* **3**, 280-291.

Jensen, K. J., Alpini, G. and Glaser, S. (2013). Hepatic nervous system and neurobiology of the liver. *Compr. Physiol.* **3**, 655-665.

Kaneko, K., Kamimoto, K., Miyajima, A. and Itoh, T. (2015). Adaptive remodeling of the biliary architecture underlies liver homeostasis. *Hepatology* **61**, 2056-2066.

Kato, H. and Shimazu, T. (1983). Effect of autonomic denervation on DNA synthesis during liver regeneration after partial hepatectomy. *Eur. J. Biochem.* **134**, 473-478.

Knosp, W. M., Knox, S. M., Lombaert, I. M. A., Haddox, C. L., Patel, V. N. and Hoffman, M. P. (2015). Submandibular parasympathetic gangliogenesis requires sprouty-dependent Wnt signals from epithelial progenitors. *Dev. Cell* **32**, 667-677.

Li, W., Kohara, H., Uchida, Y., James, J. M., Soneji, K., Cronshaw, D. G., Zou, Y.-R., Nagasawa, T. and Mukouyama, Y.-S. (2013). Peripheral nerve-derived CXCL12 and VEGF-A regulate the patterning of arterial vessel branching in developing limb skin. *Dev. Cell* **24**, 359-371.

Lu, P. and Werb, Z. (2008). Patterning mechanisms of branched orga. *Science* **322**, 1506-1509.

Nedvetsky, P. I., Emmerson, E., Finley, J. K., Ettinger, A., Cruz-Pacheco, N., Prochazka, J., Haddox, C. L., Northrup, E., Hodges, C., Mostov, K. E. et al. (2014). Parasympathetic innervation regulates tubulogenesis in the developing salivary gland. *Dev. Cell* **30**, 449-462.

Oben, J. A. and Diehl, A. M. (2004). Sympathetic nervous system regulation of liver repair. *Anat. Rec. A Discov. Mol. Cell. Evol. Biol.* **280**, 874-883.

Peters, R. J., Osinski, M. A., Hongo, J.-A., Bennett, G. L., Okragly, A. J., Haak-Frendscho, M. and Epstein, M. L. (1998). GDNF is abundant in the adult rat gut. *J. Auton. Nerv. Syst.* **70**, 115-122.

Senga, K., Mostov, K. E., Mitaka, T., Miyajima, A. and Tanimizu, N. (2012). Grainyhead-like 2 regulates epithelial morphogenesis by establishing functional tight junctions through the organization of a molecular network among claudin3, claudin4, and Rab25. *Mol. Biol. Cell* **23**, 2845-2855.

Seseke, F. G., Gardemann, A. and Jungermann, K. (1992). Signal propagation via gap junctions, a key step in the regulation of liver metabolism by the sympathetic hepatic nerves. *FEBS Lett.* **301**, 265-270.

Shimazu, T. and Amakawa, A. (1968). Regulation of glycogen metabolism in liver by the autonomic nervous system. 3. Differential effects of sympathetic-nerve stimulation and of catecholamines on liver phosphorylase. *Biochim. Biophys. Acta* **165**, 349-356.

Shimazu, T. and Fukuda, A. (1965). Increased activities of glycogenolytic enzymes in liver after splanchnic-nerve stimulation. *Science* **150**, 1607-1608.

Tanimizu, N., Saito, H., Mostov, K. and Miyajima, A. (2004). Long-term culture of hepatic progenitors derived from mouse Dlk+ hepatoblasts. *J. Cell Sci.* **117**, 6425-6434.

Tanimizu, N., Kobayashi, S., Ichinohe, N. and Mitaka, T. (2014). Downregulation of miR122 by grainyhead-like 2 restricts the hepatocytic differentiation potential of adult liver progenitor cells. *Development* **141**, 4448-4456.

Tanimizu, N., Kaneko, K., Itoh, T., Ichinohe, N., Ishii, M., Mizuguchi, T., Hirata, K., Miyajima, A. and Mitaka, T. (2016). Intrahepatic bile ducts are developed through formation of homogeneous continuous luminal network and its dynamic rearrangement in mice. *Hepatology* **64**, 175-188.

Ueno, T., Bioulac-Sage, P., Balabaud, C. and Rosenbaum, J. (2004). Innervation of the sinusoidal wall: regulation of the sinusoidal diameter. *Anat. Rec. A Discov. Mol. Cell. Evol. Biol.* **280**, 868-873.